Ocean Engineering 259 (2022) 111909

Contents lists available at ScienceDirect

Ocean Engineering

journal homepage: www.elsevier.com/locate/oceaneng

Using ANN to study VIV of flexible cylinders in uniform and shear flows

Jixiang Song [a,b,c], Weimin Chen [a,b,*], Shuangxi Guo [a,b], Dingbang Yan [a,b,d]

[a] Key Laboratory for Mechanics in Fluid-Solid Coupling Systems, Institute of Mechanics, Chinese Academy of Science, Beijing, 100190, PR China
[b] School of Engineering Science, University of Chinese Academy of Sciences, Beijing, 100049, PR China
[c] State Key Laboratory of Simulation and Regulation of Water Cycle in River Basin, China Institute of Water Resources and Hydropower Research, Beijing, 100038, China
[d] College of Mechanical and Electrical Engineering, Hunan Applied Technology University, Changde, Hunan, 415100, China

ARTICLE INFO

Keywords:
Flexible cylinder
Vortex-induced vibration
Neural network

ABSTRACT

The ANN model trained on experimental datasets is developed, especially based on the characteristics of flexible cylinder's VIV, the Bayesian regularization back propagation algorithm is employed to train the presented neural network. Nine intuitive physical parameters are selected according to the governing equations of cylinder dynamics. The results show that the neural network trained with intuitive physical quantity can acceptable predictions predict VIV, and the linear regression value is 0.940. In addition, the range of model parameters is limited in the trained neural network, with around 20% error.

1. Introduction

The Vortex-Induced Vibrations (VIV) of cylinders are a widely occurring complex fluid-structure coupling phenomenon and can cause rapid fatigue failure. The flexible cylinder VIV in ocean currents is multi-mode characterized by broad-band random vibration since flexible cylinders have lower-frequency and higher-density natural modes. Moreover, the extended cylinder vibration patterns are standing waves or traveling waves. In the past few decades, semi-empirical wake oscillation method, modal superposition method, and the numerical simulation CFD method have been used to predict VIV. However, the semi-empirical method is that the parameters are based on the cylindrical forced vibration experiment, while the computational efficiency of numerical simulation CFD is low, and large Reynolds numbers (10^6) cannot be calculated.

To reveal the mechanism of the VIV phenomenon, researchers have done many experiments (Sarpkaya, 2004; C.H.K. Williamson and Govardhan, 2004; C. H. K. Williamson and Govardhan, 2008). They got some parameters that affect the VIV phenomenon, such as Reynolds number, mass ratio, Strouhal number, and reduction speed (J. K. Vandiver, 1993). However, these parameters cannot be satisfied simultaneously in experiments, such as the Reynolds number *Re* and Froude number *Fr*. According to the research content, the researchers choose basic parameters based on a priori experience while ignoring other parameters (Erling Huse, 1996; E. Huse, Kleiven and Nielsen, 1998). However, there is a complicated nonlinear relationship between the parameters. In some cases, the neglected parameters have a non-negligible impact on the VIV phenomenon (Ren et al., 2011). Therefore, the choice of parameters is a challenge.

As we know, the prediction methods of flexible cylinder VIV include semi-empirical wake oscillator, modal superposition (frequency domain or time domain) method and numerical simulation CFD method. However, in the numerical simulation CFD, the Reynolds number Re reaches 106, the calculation accuracy decreases and the calculation cost is large. The semi-empirical methods are based on mostly the forced vibration experiment of rigid cylinder and use priori and even posteriori parameters to predict cylinder VIV, e.g., the mode advantage factor κcf. To solve the problems of computational efficiency, posterior parameter, and parameters selection, we will use ANN to predict flexible cylinder VIV. Actually, ANN has been applied to solve VIV problems due to its better ability of dealing with highly nonlinear traits of VIV (Liu et al., 2021; Wong et al., 2018; Xiros and Aktosun, 2022), as well as other fluid-structure interaction problems (Chen et al., 2008; Jain and Deo, 2006; Saeed et al., 2013; Song et al., 2018; Zhang et al., 2020). Wong and Kim (2018) proposed a simplified approach to predict VIV fatigue damage of top tensioned riser (TTR) based on ANN. The VIV fatigue damage was calculated from a total of 21,532 riser models by SHEAR7. The results showed that the final ANN model can predict fatigue damage well using shorter computational time, compared with the conventional semi-empirical methods. Liu et al. (2021) developed an optimal design

* Corresponding author. Key Laboratory for Mechanics in Fluid-Solid Coupling Systems, Institute of Mechanics, Chinese Academy of Science, Beijing, 100190, PR China.
E-mail address: wmchen@imech.ac.cn (W. Chen).

https://doi.org/10.1016/j.oceaneng.2022.111909
Received 18 August 2020; Received in revised form 15 June 2022; Accepted 3 July 2022
Available online 14 July 2022

method based on the data-driven model and genetic algorithm (GA), and then, to design the fairing to suppress cylinder VIV. The method can be efficiently performed by 2D-CFD calculations, and the amplitude of cylinder VIV can be significantly reduced. However, the datasets essentially came from numerical calculations, instead of the experimental VIV datasets, that might be the reason why there were somewhat errors between the predicted values and the actual situations. Ma, Resvanis, and Vandiver (2020) proposed a weighted sparse-input neural network (WSPINN) where the prior physical knowledge about VIV was principally employed to constrain neural network optimization. They identified five important physical features, i.e. Reynolds number, damping parameter, shear parameter, mode advantage factor and in-line response amplitude, that most significantly affect flexible cylinders' cross-flow vibration amplitude, among seventeen dimensionless physical features. Because some features, such as the damping parameter and mode advantage factor, are unknown before VIV experiment, which might not conducive to accurate VIV prediction.

Therefore, to avoid posterior parameters and to use experimental datasets instead of numerical datasets, in this study, we alternatively propose some intuitive physical quantities to train the ANN so as to rationally predict cylinder VIV. Nine intuitive physical quantities are chosen based on the governing equations of a cylinder dynamics. These intuitive physical quantities can intuitively predict cylinder VIV compared to many dimensionless parameters. Furthermore, this approach avoids the use of unknown posterior parameters and can simplify the processing of experimental data. On the trained ANN, the impacts of some important parameters on VIV are also analyzed.

The paper is structured as follows. In Section 2, the main characteristics of ANNs that consider VIV will be outlined. Bayesian regularization backpropagation algorithms are selected to train ANN. In Section 3, VIV is predicted based on the VIVDR Dataset. Furthermore, the influence of different ANN network structures on the prediction results is tested. The error between prediction and experiment is analyzed in Section 4. The model parameter range predicted by the trained neural network is given. When the two model parameters change, and other variables remain unchanged, the influence of the parameters on the predicted cross-flow amplitude is studied. The conclusions are drawn in Section 5.

2. Prediction of VIV

2.1. Flexible cylinder VIV modeling

The governing differential equation of cylinder dynamics is (How et al., 2009)

$$EI\frac{\partial^4 y(z,t)}{\partial z^4}-T\frac{\partial^2 y(z,t)}{\partial z^2}+m_z\frac{\partial^2 y(z,t)}{\partial t^2}+c\frac{\partial y(z,t)}{\partial t}-f(z,t)=0 \tag{1}$$

where y represents the cross-flow displacement of the cylinder. z represents the length position. t is the time. EI, T, m_z are the bending stiffness, the tension, and the uniform mass per unit length of the cylinder (including the cylinder mass m_c, inflow mass m_{in}, and additional mass $m_a = C_A m_w$), respectively. C_A is the additional mass coefficient. m_w is the drainage mass per unit length of the cylinder. c is the structural damping coefficient. $f(z,t)$ represents the transverse force per unit length.

The ocean current acts on the three-dimensional cylinder, and the external load generated is divided into two parts: the in-line drag force $F_D(z,t)$ and the oscillating lift $F_L(z,t)$ (Blevins, 1977; Faltinsen, 1990). $F_D(z,t)$ is comprised of a mean drag term and a harmonic drag.

$$F_D(z,t)=\frac{1}{2}\rho C_D(z,t)U^2(z)D+A_D\cos(4\pi f_v t+\varphi_1) \tag{2}$$

where $C_D(z,t)$ is the spatially timely-varying drag coefficient. A is the displacement. D is diameter of cylinder. ρ is the water density. U (z) is the velocity of current. A_D is the amplitude of the harmonic part of the drag force. φ_1 is the phase angles. $F_L(z,t)$, normal to $F_D(z,t)$, can be expressed as

$$F_L(z,t)=\frac{1}{2}\rho C_L(z,t)U^2(z)D\cos(2\pi f_v t+\varphi_2) \tag{3}$$

where $C_L(z,t)$ is the spatially timely-varying lift coefficient. φ_2 is the phase angles. f_v, the non-dimensional vortex shedding frequency, can be expressed as

$$f_v=\frac{S_t U}{D} \tag{4}$$

where S_t is the Strouhal number, and it usually takes the value of 0.2.

In forced vibration experiments, Cross-flow excitation coefficient $C_L(z,t)$ is the function A^*_{CF} and $f_{r,CF}$, as shown in Fig. 1 (Gopalkrishnan, 1993). A^*_{CF} is the cross-flow non-dimensional amplitude A/D respectively, $f_{r,CF}=f_{CF}D/U$ is the non-dimensional frequency, f_{CF} is lock-in frequency. Furthermore, Fig. 2 shows that the added mass of the riser is not a fixed value in the VIV system (Xue et al., 2014). It can be seen that in self-excited vibration, the VIV phenomenon is more complicated.

2.2. Choose the parameters to participate in VIV

Scientific research prefers to use dimensionless equations because dimensionless equations are universal. Furthermore, according to the prior experience, the most important parameter affecting VIV is known as the Reynolds number, defined as Re=UD/ν, where: U is the relative velocity of the flowing fluid experienced by the cylinder, and ν is the kinematic viscosity of the fluid, which is 10^{-6} m^{-2}/s used in the paper. The second important parameter affecting VIV is known as the mass ratio, defined as $m^* = 4m_z/(\pi\rho D^2)$, where m_z is mass per unit length, including the mass of the cylinder itself and the mass of inflow.

From the governing differential equation of cylinder dynamics Eq. (1), we know that the dimensional parameters EI, T, m_z, c, $f(z,t)$, L (the entire length of the cylinder), length position z, control the dynamic displacement y of cylinder.

$$y(z,t)=F(EI,T,m_z,c,f(z,t),L,z) \tag{5}$$

The spatiotemporal root-mean-square (RMS) amplitude of cross-flow vibration $y_{RMS,CF}$ is the target output, taking into account the influence of Reynolds number, mass ratio, gravity, changes in flow velocity, and vibration displacement in the downstream direction on the vibration displacement in the transverse direction, the predictive model can be expressed as,

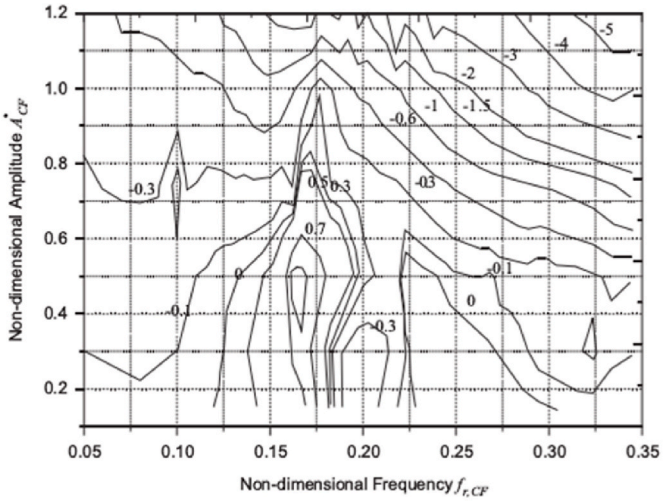

Fig. 1. Cross-flow excitation coefficient $C_L(z,t)$.

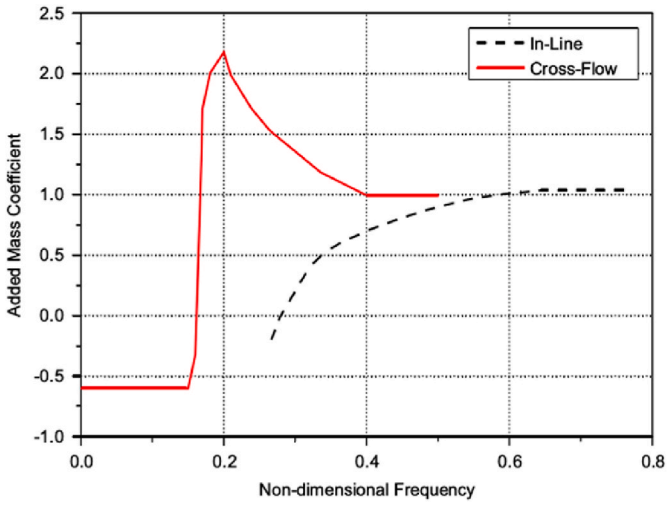

Fig. 2. Added mass coefficient C_A for CF- and IL-VIV.

$$y_{RMS,CF} = F\left(EI, T_{RMS,T}, T_{RMS,B}, U_{RMS,T}, U_{RMS,B}, m_z, c, f(z,t), L, z, \mathrm{Re}, m^*\right) \quad (6)$$

where $T_{RMS,T}$ is the RMS of tension at the top cylinder, $T_{RMS,B}$ is the RMS of tension at the bot cylinder, $U_{RMS,T}$ is the RMS of velocity at the top cylinder, $U_{RMS,B}$ is the RMS of velocity at the bot cylinder. Usually, only the Reynolds number *Re* with the highest flow velocity at the top of the riser is selected, and the additional mass coefficient $C_A = 1$. But in fact, the Reynolds number *Re* and additional mass coefficient change along the length of the cylinder and time.

The structural damping coefficient *c* has the following forms:

$$c_i = 2m_z w_i \zeta \quad (7)$$

$$w_i = \frac{i\pi}{L}\sqrt{\left(\frac{i\pi}{L}\right)^2 \frac{EI}{m_z} + \frac{T_{equ}}{m_z}} \quad (8)$$

where T_{equ} represents equivalent tension, controlled by $T_{RMS,T}$, $T_{RMS,B}$, self-weight. w_i represents frequency of the i-th mode, *i* is the mode order. The structural damping ratio ζ in the experiment was around 0.5% (J. Kim Vandiver et al., 2018).

Further simplification Eq. (6), removing unnecessary duplicate parameters, available as follows

$$y_{RMS,CF} = F\left(EI, T_{RMS,T}, T_{RMS,B}, U_{RMS,T}, U_{RMS,B}, m_z, D, L, z\right) \quad (9)$$

So Nine intuitive physical quantities, i.e. the bending stiffness *EI*, RMS of tension at the top cylinder $T_{RMS,T}$, RMS of tension at the bot cylinder $T_{RMS,B}$, RMS of velocity at the top cylinder $U_{RMS,T}$, RMS of velocity at the bot cylinder $U_{RMS,B}$, uniform mass per unit length of the cylinder m_z, diameter of cylinder *D*, entire length of the cylinder *L* and the length position *z*, are used to predict vibration displacement of the cylinder $y_{RMS,CF}$. However, Eq. (9) only apply to the VIV under uniform flow and shear flow, but not for gradient flow and other non-uniform flows.

2.3. Artificial neural network based on experimental data

The dataset is from VIVDR Dataset 8 and Dataset 10 (VIVDR, 2008). This paper only focuses on the VIV phenomenon of bare cylinders, ignoring the cylinder data with Strakes. In Dataset 8, the cylinder model is 9.63-m-long and was made of a brass pipe with an outer diameter of 20 mm and a wall thickness of 0.45 mm. The model was tested in uniform and linearly shear current profiles with the maximum flow speed, U_{max}, ranging from 0.2 m/s to 2.38 m/s. The time history curve of velocity and displacement of test no.1212 are shown in Fig. 3 and Fig. 4, respectively. The flow velocity between the two blue lines is intercepted

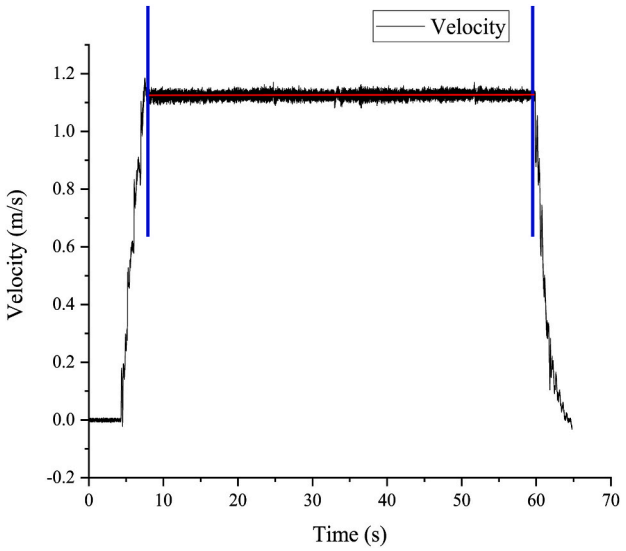

Fig. 3. Time history curve of velocity of test no.1212.

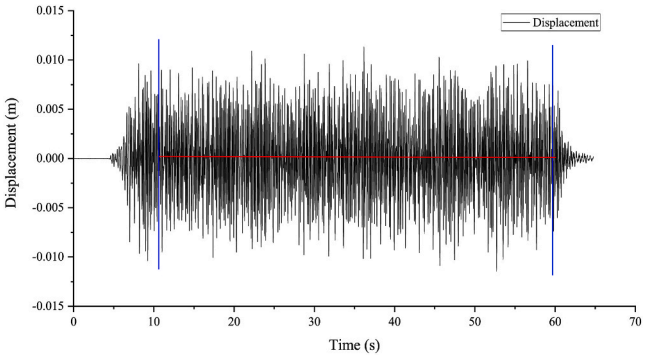

Fig. 4. Time history curve of cross-flow displacement of test no.1212 at 6.42 m.

and RMS calculation is performed to obtain the U_{RMS}. The Reynolds number *Re* ranges from 4.0×10^3–4.76×10^4. Unfortunately, in some tests, Fz_bot is not good.

$$T_{RMS,B,j} = \overline{F}_{RMS,Z\_bot,j} = F_{RMS,Z\_top,j} - \frac{1}{n}\sum_{i=1}^{n}\left(F_{RMS,Z\_top,i} - F_{RMS,Z\_bot,i}\right)^2 \quad (10)$$

where $T_{RMS,B,j}$ is the RMS of tension at the bot cylinder, is equal to $\overline{F}_{RMS,Z\_bot,j}$ (the RMS of tension at the bot cylinder in dataset). $F_{RMS,Z\_top,j}$ is the RMS of velocity at the top cylinder. *j* is the serial number of the test to be corrected Fz_bot, and $i = 1,2,3 \ldots, n$ is the total number of experiments with reasonable results. Through such simple processing, good results have been obtained.

In Dataset 10, the cylinder model is 38-m-long and an outer diameter of 27 mm. The model was tested in uniform and linearly shear current profiles with the maximum flow speed U_{max}, 0.7 m/s, and 1.4 m/s, respectively. This resulted in the Reynolds number *Re* is 1.89×10^4, and 3.78×10^4. The dimension and order of magnitude of the parameters are not consistent, so normalization is carried out.

The total number of data is 416, and partial data are shown in Table 1. Nine intuitive physical quantities are the input parameters of ANN, and vibration displacement of the cylinder $y_{RMS,CF}$ is the output parameter of ANN according to Eq. (9). 85% of the experimental data were randomly selected as the training data, while the rest was used as the test data. The number of hidden layers and nodes of the neural network has a significant influence on training the neural network. There is no effective way to design a neural network structure

Table 1
Partial data in 416 groups.

Input									Output
EI	$T_{RMS,T}$	$T_{RMS,B}$	$U_{RMS,T}$	$U_{RMS,B}$	m_z	D	L	z	$y_{RMS,CF}$
135.4	694.45	653.89	0.282	0.282	0.699	0.02	9.63	6.42	0.0062
135.4	717.77	698.14	0.831	0.831	0.699	0.02	9.63	2.14	0.0027
135.4	525.09	483.80	1.624	1.624	0.699	0.02	9.63	1.07	0.0073
135.4	611.72	570.43	2.243	2.243	0.699	0.02	9.63	1.07	0.0041
135.4	691.94	649.77	0.494	0.000	0.699	0.02	9.63	2.14	0.0057
135.4	710.42	669.13	1.263	0.000	0.699	0.02	9.63	8.56	0.0064
16.1	4090.70	4084.71	1.389	1.389	0.197	0.012	38	16.89	0.0111
16.1	3871.92	3663.58	0.692	0.000	0.197	0.012	38	13.68	0.0087
16.1	3871.92	3663.58	0.692	0.000	0.197	0.012	38	33.01	0.0108
16.1	4219.50	4216.38	1.683	1.683	0.197	0.012	38	28.86	0.0105
135.4	523.08	481.79	1.865	1.865	0.699	0.02	9.63	3.21	0.0080

(Karsoliya, 2012; Vujicic et al., 2016). Therefore, this paper constructs different hidden layer numbers and hidden layer neurons for comparative analysis, as shown in Table 2. Since the weight initialization of the neural network is random, the neural network trained will be different each time. If the trained neural network cannot generate good results, the network can be retrained.

The Mean squared error and Regression for the configurations of the models are compared. ANN-1∼ANN-5 have one hidden layer with different numbers of neurons. In addition, MSE is almost no different. However, as the number of neurons increases, the regression value decreases, below 0.75, and even the minimum value is 0.422. Due to insufficient training, this is an "underfit" training set. In comparison, ANN-6∼ANN-9 have two hidden layers with different numbers of neurons. The ANN adapts too much (or overfits) to the training set, like ANN-7, and ANN-9, the other test cases are in general the errors are large. The Training MSE is litter than Test MSE, and the Training Regression is larger than Test Regression in ANN-7, and ANN-9.

Among the nine models, ANN-6 is the best because the difference between Training MSE and Test MES is small, and Training regression and Test regression are both higher than 0.9, and the difference is minimal. This model can predict the training set and test set well and has a certain generalization ability. Fig. 5 shows the Neural Network Regression of ANN-6, which is the closest to 1. Therefore, it is not difficult to conclude that compared with many dimensionless parameters (Ma et al., 2020), intuitive physical quantities with fewer parameters can intuitively predict VIV.

3. Predictions of VIV vs experiments of VIV

Due to the limited amount of experimental data and the small coverage of the parameters, a trained neural network can only make accurate predictions within a limited range. We use the neural network trained by the ANN-6 model to analyze the flexible cylinder VIV responses.

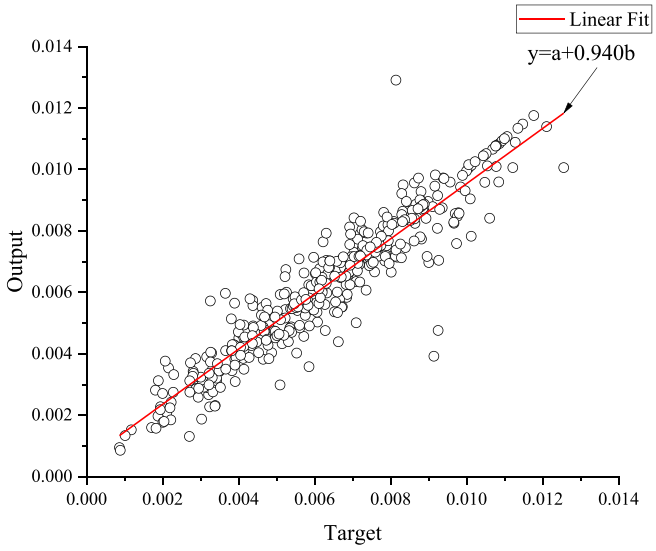

Fig. 5. Neural network regression.

3.1. Errors between predictions and experiments

The errors between predictions and experiments have been analyzed through test no.1115 and test no. 1214 in Dataset 8. Fig. 8 and Fig. 9 are RMS displacement of eight different positions on the riser under different working conditions. The predicted displacement is close to the experimental displacement, and the maximum displacement difference is only 0.0014 m ($z = 3.21$ m in Fig. 6). Except one error of −38% ($z = 2.14$ m in Fig. 7), most errors are between −19% ∼ 22%, i.e. the errors are −12%∼22% in uniform flow and the errors are −38%–14% in shear flow. It can be seen that the predicted displacement is effective.

Table 2
Architecture of the multilayer ANN.

Configuration	Hidden layer	Neurons	Training Mean squared error	Training Regression	Test Mean squared error	Test Regression
ANN-1	1	10	2.74e-06	0.726	4.02e-06	0.544
ANN-2	1	15	4.50e-06	0.461	4.08e-06	0.550
ANN-3	1	20	4.39e-06	0.484	4.86e-06	0.422
ANN-4	1	25	4.55e-06	0.476	3.72e-06	0.473
ANN-5	1	30	4.61e-06	0.468	3.36e-06	0.531
ANN-6	2	20–5	4.42e-06	0.943	2.28e-06	0.901
ANN-7	2	20–10	1.62e-07	0.986	4.64e-05	0.342
ANN-8	2	20–15	2.26e-08	0.763	4.12e-06	0.700
ANN-9	2	20–20	4.42e-09	1.000	1.85e-06	0.345

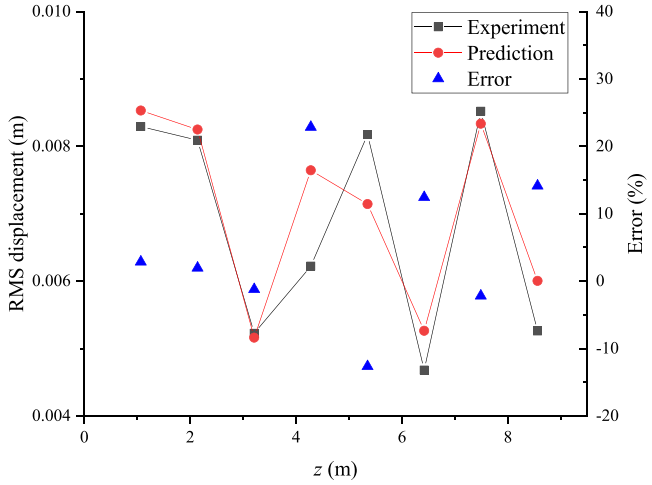

Fig. 6. Prediction and experiment RMS displacement of VIV in test no.1115 in Dataset 8 in uniform flow.

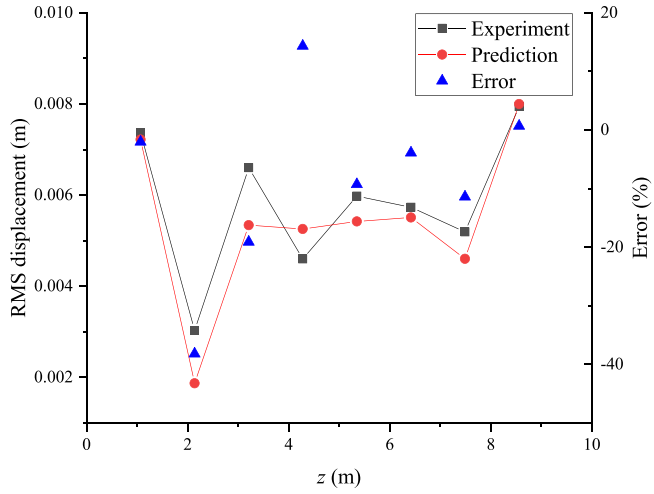

Fig. 7. Prediction and experiment displacement of VIV in test no.1214 in Dataset 8 in shear flow.

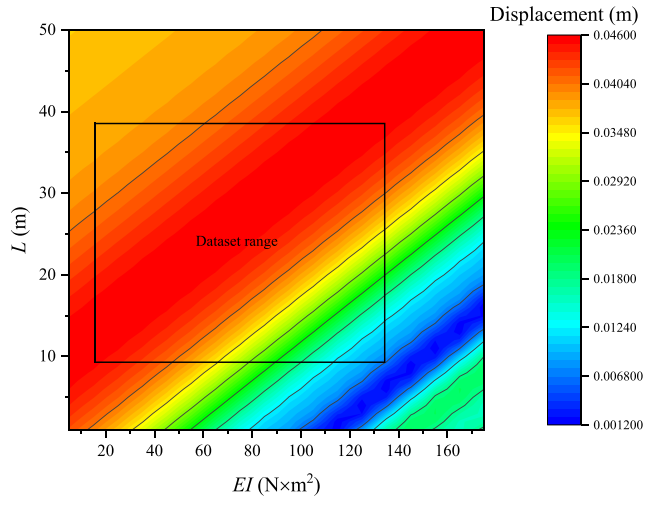

Fig. 8. Contours of RMS displacement as a function of *EI* and *L* in uniform flow.

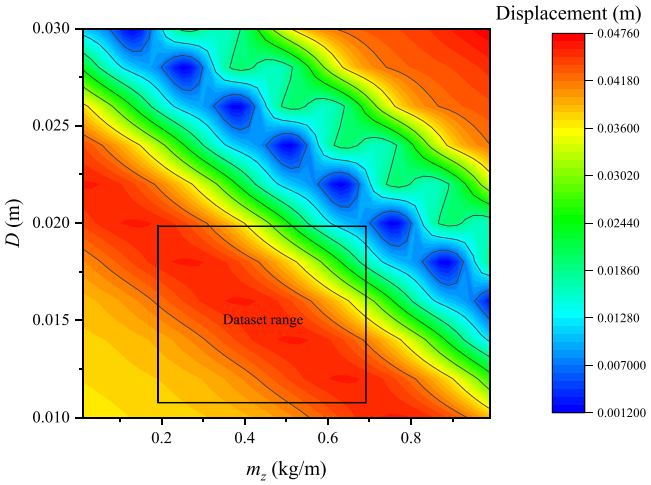

Fig. 9. Contours of RMS displacement as a function of m_z and D in uniform flow.

3.2. Model parameter range in ANN

In this section, the analysis flexible cylinder VIV response within the parameter range of trained ANN is presented. In uniform flow, the cross-flow displacement of test no.1108 in Dataset 8 at 1.070 m is selected for our analysis. The contours of RMS displacement, as a function of *EI* and *L*, are plotted in Fig. 8. In other words, *EI* and *L* are variable, and the other parameters are constant. In the dataset range, *EI* and *L* are between (16.1, 135.4) N × m2 and (9.63, 38) m, respectively, and all of the displacements are greater than zero. The maximum displacement and the minimum displacement are easy to find. The former is about four times the latter. When the L is constant, the increase in *EI* causes the displacement to increase to the peak first and then decrease. When the *EI* is constant, the same phenomenon exists. This is the opposite of what we expected (*L* is proportional to displacement). The upper left triangle (upper left of the red outline of the maximum displacement) shows that the displacement decreases slowly with the increase of *L*. The lower right triangle (the bottom right of the maximum displacement red outline) shows that the displacement decreases rapidly with the increase of *EI*. However, when *EI* exceeds a critical value, the displacement increases again. It can be seen that VIV is a complex fluid-solid coupling phenomenon.

Interestingly, the displacement contour lines are parallel at an oblique angle. In other words, the displacement of any (*EI*, *L*) points can be replaced by other (*EI*, *L*) points passing through this line, which helps the design of small-scale experimental models.

The contours of RMS displacement as a function of m_z and D are shown in Fig. 9. In Dataset range, m_z and *D* are between (0.197, 0.699) kg/m and (0.012, 0.02) m, respectively. Furthermore, all the displacements are greater than zero. As the *D* increases, the displacement first increases, then decreases, and then increases. In the process of m_z increase, there are similar situations. Moreover, the displacement contour lines are no longer parallel at an oblique angle. The contour of the smallest displacement presents an irregular circle with the same spacing, which is interesting.

In shear flow, the cross-flow displacement of test no.2350 in Dataset 10 at 4.155 m is selected for analysis. The contours of RMS displacement as a function of *EI* and *L*, and other parameters are constants, as plotted in Fig. 10. The Dataset range is the same as in Fig. 8. The displacement increases rapidly with the increase of *EI*. The displacement decreases rapidly with the increase of *L*, which is different from Fig. 8. As the length increases, the natural frequency of the cylinder decreases according to Eq.(21). The vortex shedding frequency is close to the natural frequency of the cylinder, which will cause VIV lock and increase the

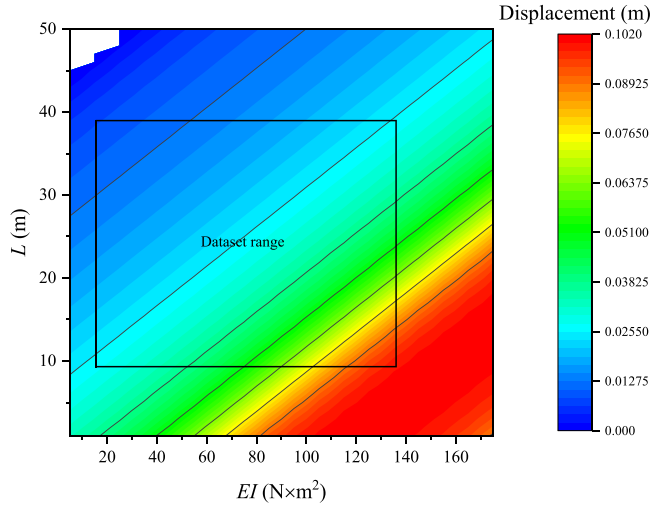

Fig. 10. Contours of RMS displacement as a function of *EI* and *L* in shear flow.

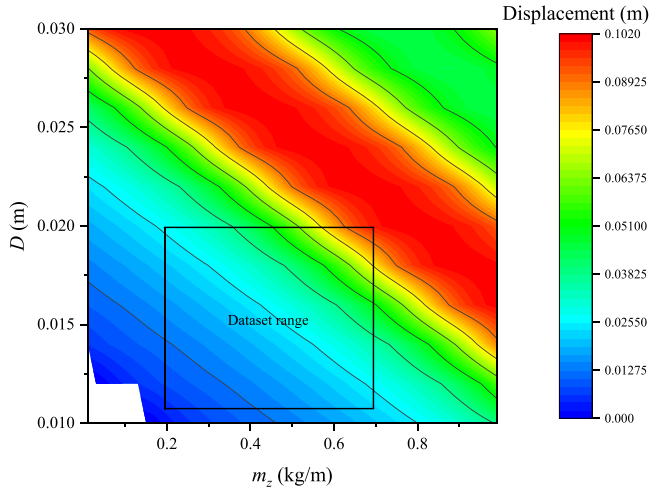

Fig. 11. Contours of RMS displacement as a function of m_z and *D* in shear flow.

displacement. The flow vortex shedding frequency is distributed along the entire length of the cylinder, the uniform flow shedding frequency is equal, while the shear flow shedding frequency is variable. The maximum vortex shedding frequency is at the maximum speed at the top, and the minimum vortex shedding frequency is 0 at the bottom. The vortex shedding frequency gradually decreases from the top to the low end and is highly dense. As a result, the shear flow has coexistence and competition of multi-modal VIV. This may be the reason why the displacement decreases as the length increases.

The white part indicates that the predicted displacement value is less than 0, which is unreasonable. This shows that the parameter range of the trained neural network is limited when predicting.

Fig. 11 shows the effect of varying m_z and *D* on displacement. The displacement decreases with the increase of m_z or *D*. When the diameter is constant, the displacement decreases nonlinearly with the increase of m_z. The possible reason is that m_z has changed the natural frequency, causing the VIV lock frequency to change. When the mass is constant, the displacement increases significantly as the diameter increases.

From the above analysis and discussion, it can be seen that the neural network trained with experimental data is acceptable in predicting VIV (around 20% error), and the influences of key parameters on VIV can be studied within a specific range. In other words, when the range of parameters for training the neural network is broad enough, it can cover the existing VIV in actual engineering. This approach helps estimate VIV in experimental design and preliminary engineering design.

4. Conclusion

The VIV of flexible cylinder's in uniform and shear flows is predicted by the developed ANN. The neural network trained with the physical parameters can effectively predict VIV, while it avoids the processing of many parameters along with possible data missing and truncation during processing. According to the characteristics of cylinder VIV, the Bayesian regularization backpropagation algorithms are chosen to train our neural network. We found that it is important to carefully compare and analyze different neural network structures before built a proper neural network structure, which may influence the prediction results. Here, different neural network structures are tested to VIV predictions. Finally, the impacts of parameter changes on VIV according to the trained neural network are examined. The main conclusions can be summarized as follows: 1) The Bayesian regularization backpropagation algorithms are more suitable for VIV prediction mainly because of highly nonlinearities of flexible cylinder VIV and inevitable errors coming from experimental results. 2) Nine intuitive physical quantities are recommended to predict cylinder VIV based on governing equations of cylinder dynamics. It is worthwhile to pointed out that the range of model parameters is limited in the trained neural network, with around 20% error.

CRediT authorship contribution statement

Jixiang Song: Conceptualization, Methodology, Writing – original draft. **Weimin Chen:** Writing – review & editing, Funding acquisition, Supervision. **Shuangxi Guo:** Visualization, Writing – original draft, Investigation. **Dingbang Yan:** Writing – original draft, Data curation.

Declaration of competing interest

The authors declare that they have no known competing financial interests or personal relationships that could have appeared to influence the work reported in this paper.

Acknowledgments

This work is supported by the Strategic Priority Research Program of the Chinese Academy of Sciences (Grant No. XDA22000000).

Appendix

Artificial neural network (ANN) model

The ANN is a reliable method to approximate the target value, which has been widely used in pattern recognition, classification, clustering, and time series (Widrow et al., 1994). The ANNS imitates biological neural networks, a learning system composed of a complex network of interconnected simple units (neurons). Each unit performs relatively simple operations separately; however, their interconnection provides a variety of tasks. Fig. 1 shows an artificial model of the neuron-McCulloch-Pitts neuron (McCulloch and Pitts, 1943). When receiving a given number of inputs x_i, $i = 1, 2, \ldots,$

N, each neuron first uses the synaptic weights w_i to calculate the linear combination of inputs to generate a weighted input z. Next, it provides the output y through the activation function $f(z)$, which must exhibit increasing monotonicity within the specific value range of z and assume constants outside this range.

$$z = \sum_{i=1}^{N} w_i x_i \tag{A.1}$$

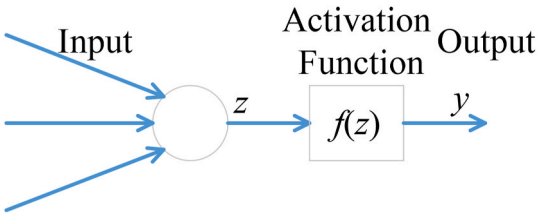

Fig. 12. McCulloch-Pitts neuron

Because the sigmoid functions are smooth, and differentiable at all points, with superior and inferior limits, they are continuous activation functions widely used in ANN applications. Several types of sigmoid functions are the logistic function and the tangent function. The tangent function will be employed in the developments presented in this work. This function is expressed by (Vogl et al., 1988):

$$y = f(z) = \frac{2}{1 + e^{-2z}} - 1 \tag{A.2}$$

Eq. (A.2) is mathematically equivalent to tanh(z). Although there are minimal differences in numerical results, the calculation speed is faster than tanh. For ANNs, this function is a good tradeoff because speed is essential, but the exact shape of the transfer function is not.

Substituting Eq. (A.1) to Eq. (A.2), an expression for the output y_j of the jth hidden neuron may be defined as follows,

$$y_j = \frac{2}{1 + e^{-2\sum_{i=1}^{N} w_i x_i}} - 1 \tag{A.3}$$

Similarly, an expression for the network output $\hat{y}$ can be obtained, taking into account the particular architecture with 20 hidden neurons:

$$\hat{y} = \sum_{j=1}^{20} w_{jo} \left(\frac{2}{1 + e^{-2\sum_{i=1}^{N} w_i x_i}} - 1 \right) \tag{A.4}$$

where w_{jo} is the weight between the wavelon j and the output.

Taking $y = (y_1, y_2, y_3, \ldots, y_n)$ as the set of desired outputs, the error E_r is given by:

$$E_r = \frac{1}{2} \sum_{k=1}^{n} (y_k - \hat{y}_k)^2 \tag{A.5}$$

where 1/2 is to eliminate the coefficient two after E_r derivative and simplify the algorithm.

Training the ANN refers to the process of adjusting the weight value w_i of the equation so that the error is sufficiently small. Mean square error (MSE) is the most commonly used neural network optimization objective function, and this function is also used in this paper. MSE is minimized at each iteration of the training procedure by adjusting the weights proportionally to the derivative of the error function with w_{ji} (t).

Bayesian regularization backpropagation algorithms can produce useful generalizations for difficult, small, or noisy data sets. Although it requires more time than Levenberg-Marquardt backpropagation, it can be tolerated for complex VIV problems. This algorithm objective function adds term, becomes (Foresee and Hagan, 1997)

$$F = \alpha E_W + \beta E_D \tag{A.6}$$

where E_D is E_r, E_w is the sum of the square of the network weights, α and β are objective function parameters. If $\alpha \ll \beta$, then the training algorithm will drive the errors smaller. If $\alpha \gg \beta$, training will emphasize weight size reduction at the expense of network errors, thus producing a smoother network response.

The density function for the weights can be expressed according to Bayes' rule:

$$P(D|\alpha, \beta, M) = \frac{P(D|w, \beta, M) P(w|\alpha, M)}{P(w|D, \alpha, \beta, M)} \tag{A.7}$$

where w is the ANN weights, D is the data set, and M is the ANN model used. $P(w|\alpha, M)$ is the prior density, which represents our knowledge of the weights before any data is collected. $P(D|w, \beta, M)$ is the likelihood function, which is the probability of the data occurring with the weights w. $P(D|\alpha, \beta, M)$ is a normalization factor, which guarantees that the total probability is 1.

Applying Bayes' rule to optimize the objective function parameters α and β. If the VIV noise in the train set data is Gaussian and the prior

distribution for the weights is Gaussian, the probability densities can be written

$$P(D|w,\beta,M)=\frac{1}{(\pi/\beta)^{n/2}}e^{-\beta E_D} \tag{A.8}$$

$$P(w|\alpha,M)=\frac{1}{(\pi/\alpha)^{n/2}}e^{-\alpha E_W} \tag{A.9}$$

Placing Eq. (A.8) and Eq. (A.9) to Eq. (A.7), we obtain

$$P(D|\alpha,\beta,M)=\frac{Z_F(\alpha,\beta)}{(\pi^2/(\alpha\beta))^{n/2}}e^{-\beta E_D-\alpha E_W+F(w)} \tag{A.10}$$

Because $Z_F(\alpha,\beta)$ is not known, we by Taylor series expansion to estimate it. Since the objective function has the shape of a quadratic in a small area surrounding a minimum point, we can expand F(w) around the minimum point of the posterior density w^{MP}, where the gradient is zero. Solving for the normalizing constant yields

$$Z_F(\alpha,\beta)\approx(2\pi)^{n/2}\left|\left(H^{MP}\right)^{-1}\right|^{1/2}e^{-F\left(w^{MP}\right)} \tag{A.11}$$

where $H=\beta\nabla^2E_D+\alpha\nabla^2E_W$ is the Hessian matrix of the objective function.

Placing Eq. (A.11) to Eq. (A.10), we obtain the optimal values for α and β at the minimum point. By taking the derivative to each log of Eq. (A.10) and setting them equal to zero. This yields

$$\alpha^{MP}=\frac{\gamma}{2E_W(w^{MP})} \tag{A.12}$$

$$\beta^{MP}=\frac{n-\gamma}{2E_D(w^{MP})} \tag{A.13}$$

where $\gamma=N-2\alpha^{MP}\mathrm{tr}(H^{MP})^{-1}$ is called the effective number of parameters, and N is the total number of parameters. This parameter γ is a measure of how many parameters in the ANN are effectively used in reducing the error function.

A two-layer feed-forward network with sigmoid hidden neurons and linear output neurons illustrated in, can fit multi-dimensional mapping problems arbitrarily well with consistent data and enough neurons in its hidden layer.

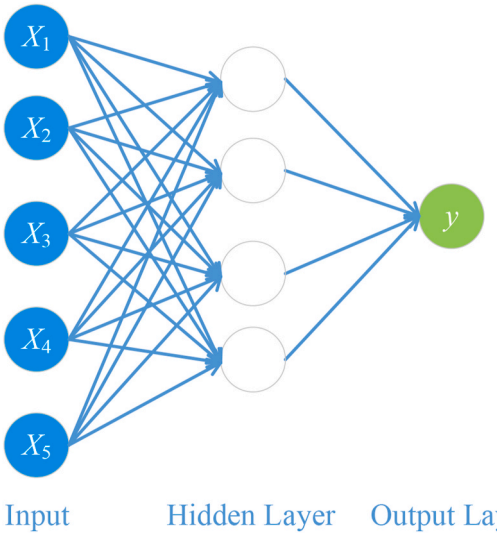

Fig. 13. A ANN example with 5 inputs and 4 neurons in the first hidden layer

References

Blevins, R., 1977. Flow-induced Vibration.

Chen, C.-H., Wu, J.-C., Chen, J.-H., 2008. Prediction of flutter derivatives by artificial neural networks. J. Wind Eng. Ind. Aerod. 96 (10), 1925–1937. https://doi.org/10.1016/j.jweia.2008.02.044.

Faltinsen, O.M., 1990. Sea Loads on Ships and Offshore Structures. Cambridge University Press, New York.

12-12 June 1997 Foresee, F.D., Hagan, M.T., 1997. Gauss-Newton Approximation to Bayesian Learning. Paper Presented at the Proceedings of International Conference on Neural Networks (ICNN'97).

Gopalkrishnan, R., 1993. Vortex-induced Forces on Oscillating Bluff Cylinders (Ph.D.). MIT, USA.

How, B.V.E., Ge, S.S., Choo, Y.S., 2009. Active control of flexible marine risers. J. Sound Vib. 320 (4), 758–776. https://doi.org/10.1016/j.jsv.2008.09.011.

Huse, E., 1996. Experimental Investigation of Deep Sea Riser Interaction. https://doi.org/10.4043/8070-MS.

Huse, E., Kleiven, G., Nielsen, F., 1998. Large Scale Model Testing of Deep Sea Risers. https://doi.org/10.4043/8701-MS.

Jain, P., Deo, M.C., 2006. Neural networks in ocean engineering. Ships Offshore Struct. 1 (1), 25–35. https://doi.org/10.1533/saos.2004.0005.

Karsoliya, S., 2012. Approximating number of hidden layer neurons in multiple hidden layer BPNN architecture. Int. J. Eng. Trends Technol. 3 (6), 714–717.

Liu, X.-q., Jiang, Y., Liu, F.-l., Liu, Z.-w., Chang, Y.-j., Chen, G.-m., 2021. Optimization design of fairings for VIV suppression based on data-driven models and genetic algorithm. China Ocean Eng. 35 (1), 153–158. https://doi.org/10.1007/s13344-021-0014-3.

Ma, L., Resvanis, T.L., Vandiver, J.K., 2020. A Weighted Sparse-Input Neural Network Technique Applied to Identify Important Features for Vortex-Induced Vibration. Paper Presented at the AAAI-MLPS 2020.

McCulloch, W.S., Pitts, W., 1943. A logical calculus of the ideas immanent in nervous activity. Bull. Math. Biophys. 5 (4), 115–133. https://doi.org/10.1007/BF02478259.

Ren, T., Fu, S., Li, R., Yang, J., 2011. Full scale riser Vortex-Induced-Vibration response prediction based on model test. J. Ship Mech. 15, 364–370. https://doi.org/10.3969/j.issn.1007-7294.2011.04.006.

Saeed, R.A., Galybin, A.N., Popov, V., 2013. 3D fluid–structure modelling and vibration analysis for fault diagnosis of Francis turbine using multiple ANN and multiple ANFIS. Mech. Syst. Signal Process. 34 (1), 259–276. https://doi.org/10.1016/j.ymssp.2012.08.004.

Sarpkaya, T., 2004. A critical review of the intrinsic nature of vortex-induced vibrations. J. Fluid Struct. 19 (4), 389–447. https://doi.org/10.1016/j.jfluidstructs.2004.02.005.

Song, L.-K., Wen, J., Fei, C.-W., Bai, G.-C., 2018. Distributed collaborative probabilistic design of multi-failure structure with fluid-structure interaction using fuzzy neural network of regression. Mech. Syst. Signal Process. 104, 72–86. https://doi.org/10.1016/j.ymssp.2017.09.039.

Vandiver, J.K., 1993. Dimensionless parameters important to the prediction of vortex-induced vibration of long, flexible cylinders in ocean currents. J. Fluid Struct. 7 (5), 423–455. https://doi.org/10.1006/jfls.1993.1028.

Vandiver, J.K., Ma, L., Rao, Z., 2018. Revealing the effects of damping on the flow-induced vibration of flexible cylinders. J. Sound Vib. 433, 29–54. https://doi.org/10.1016/j.jsv.2018.07.009.

VIVDR, 2008. Vortex Induced Vibration Data Repository. Retrieved from. http://web.mit.edu/towtank/www/vivdr/index.html.

Vogl, T.P., Mangis, J.K., Rigler, A.K., Zink, W.T., Alkon, D.L., 1988. Accelerating the convergence of the back-propagation method. Biol. Cybern. 59 (4), 257–263. https://doi.org/10.1007/BF00332914.

Vujicic, T., Matijevic, T., Ljucovic, J., Balota, A., Sevarac, Z., 2016. Comparative analysis of methods for determining number of hidden neurons in artificial neural network. In: Paper Presented at the Central European Conference on Information and Intelligent Systems.

Widrow, B., Rumelhart, D.E., Lehr, M.A., 1994. Neural networks: applications in industry, business and science. Commun. ACM 37, 93–105.

Williamson, C.H.K., Govardhan, R., 2004. Vortex-Induced vibrations. Annu. Rev. Fluid Mech. 36 (1), 413–455.

Williamson, C.H.K., Govardhan, R., 2008. A brief review of recent results in vortex-induced vibrations. J. Wind Eng. Ind. Aerod. 96 (6–7), 713–735.

Wong, E.W.C., Choi, H.S., Kim, D.K., Hashim, F.M., 2018. Development of ANN Model for the Prediction of VIV Fatigue Damage of Top-Tensioned Riser, vol. 203. MATEC Web Conf., 01013 https://doi.org/10.1051/matecconf/201820301013. Retrieved from.

Wong, E.W.C., Kim, D.K., 2018. A simplified method to predict fatigue damage of TTR subjected to short-term VIV using artificial neural network. Adv. Eng. Software 126 (DEC), 100–109.

Xiros, N.I., Aktosun, E., 2022. Stabilization of neural network models for VIV force data using decoupled, linear feedback. J. Mar. Sci. Eng. 10 (2), 272. Retrieved from. https://www.mdpi.com/2077-1312/10/2/272.

Xue, H., Tang, W., Qu, X., 2014. Prediction and analysis of fatigue damage due to cross-flow and in-line VIV for marine risers in non-uniform current. Ocean Eng. 83 (jun.1), 52–62.

Zhang, Y., Zheng, X., Xue, Q., 2020. A deep neural network based glottal flow model for predicting fluid-structure interactions during voice production. Appl. Sci. 10 (2), 705. Retrieved from. https://www.mdpi.com/2076-3417/10/2/705.